Additive Manufacturing 95 (2024) 104538

Contents lists available at ScienceDirect

Additive Manufacturing

journal homepage: www.elsevier.com/locate/addma

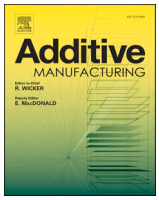

On-line inspection of lattice structures and metamaterials via in-situ imaging in additive manufacturing

Bianca Maria Colosimo [a,*], Federica Garghetti [a], Marco Grasso [a], Luca Pagani [b]

[a] Department of Mechanical Engineering, Politecnico di Milano, Via La Masa 1, Milan 20156, Italy
[b] OPEN MIND Technologies AG, Argelsrieder Feld 5, Weßling 82234, Germany

ARTICLE INFO

Keywords:
In-situ monitoring
Image
Qualification
Inspection
Lattice structures
Metamaterials
Additive manufacturing
Powder bed fusion
Data mining

ABSTRACT

As advanced production capabilities are moving towards novel types of geometries as well as higher customization demands, a new and more efficient approach for process and part qualification is becoming an urgent need in industry. The layerwise nature of additive manufacturing (AM) potentially allows anticipating qualification tasks in-line and in-process, aiming at reducing the time and costs devoted to post-process inspections, enabling at the same time an early detection of defects since their onset stage. Such opportunity is particularly attractive in the presence of highly complex shapes like lattice structures or metamaterials, which have been increasingly investigated for industrial adoption in various sectors, aiming to achieve enhanced mechanical properties and innovative functionalities. This paper presents a novel methodology to inspect the geometry of lattice structures while the part is being built. The method is specifically designed to tackle the natural variability affecting layerwise images gathered in laser powder bed fusion. To this aim, it combines the segmentation of in-situ powder bed images of solidified layers with a data modelling approach to synthesize the 3-D shape of each unit cell into a 1-D profile representation. Such low-dimensional representation is suitable to quickly detect undesired distortions that may have a detrimental impact on final quality and performance. By using post-process X-ray computed tomography as ground truth reference, this study shows the effectiveness of the proposed approach for in-line inspection, opening a novel and cost-efficient way to address complex shape qualification for lattice structures in AM.

1. Introduction

Additive Manufacturing (AM) has enabled a quick and widespread evolution from traditional product designs to full 3-dimensional (3-D) complex shapes in many real industrial applications. New levels of part complexity allow meeting new market demands, including increased customization, higher sustainability of the whole production chain and enhanced product performances, from extended life to novel embedded functionalities. Nevertheless, making use of such design freedom implies a wider adoption of advanced non-destructive inspection methodologies. The only viable solution to inspect the intricate internal features of additively manufactured parts is X-ray computed tomography (CT). It allows determining discrepancy models of both external and internal features, inspecting volumetric defects and qualifying high-value-added components. However, the adoption of X-ray CT inflates the time and cost required by quality assurance procedures, while in the presence of large parts of highly dense materials it can be even unfeasible. On the other side, an approach to detect defective products in-situ and in-line, as soon as they appear during the process can significantly reduce resource and energy waste allowing detection of nonconforming products as soon as they appear.

Aforementioned qualification challenges are even more crucial for a specific family of complex shapes enabled by AM processes, i.e., lattice structures. These structures, also known as metamaterials, are structures that inherit their functional properties from their shape rather than from the material they are composed of. They represent one of most innovative light-weight design solutions in today's industry, thanks to the advanced mechanical, thermal, and functional performances enabled by their geometrical properties, and by the highly efficient use of the material they are composed of [1,2]. The spread of lattice structures makes the lack of adequate and efficient qualification methods a relevant industrial problem. Local and internal inaccuracies may have a detrimental effect on the functional performance of the whole structure, and such inaccuracies can only be determined by means of expensive X-ray

* Corresponding author.
E-mail address: biancamaria.colosimo@polimi.it (B.M. Colosimo).

https://doi.org/10.1016/j.addma.2024.104538
Received 26 April 2024; Received in revised form 2 October 2024; Accepted 4 November 2024
Available online 6 November 2024

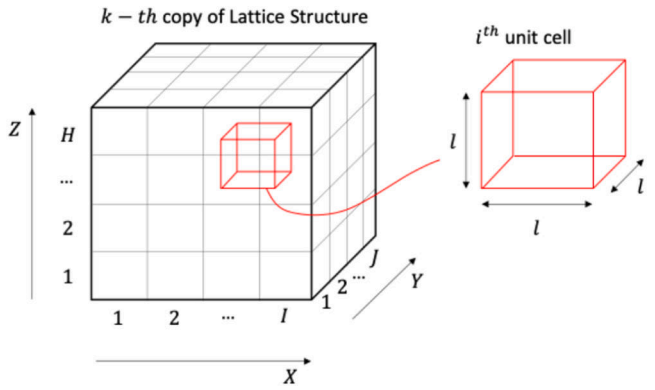

Fig. 1. Schematic view of a lattice structure envelope as a 3-D array of unit cells.

CT measurements. As an example, a local dimensional and/or geometrical mismatch between the manufactured part and the nominal geometry may worsen the mechanical properties and influence the type of failure mechanism [3]. It can also affect other functionalities, like fluid separation in heat exchangers or the osteo-integration effectiveness in biomedical applications [4].

The present study is specifically aimed at developing an approach for in-situ and in-line data modelling and inspection of lattice structures to take advantage of the layerwise AM production paradigm, to 1) anticipate the detection of possible anomalies while the part is being built, and 2) reduce the need for post-process non-destructive analysis. Despite dimensional and geometrical estimates gathered in-situ may be not fully representative of the actual size and shape of parts obtained at the end of the build – since shrinkage effects and distortions occurring *under* the layer cannot be captured – significant geometrical anomalies can be observed during the build, and should bring to an alarm, to early detect non-conformities. Indeed, in-situ measurements and monitoring have been pointed out to play a critical role towards more efficient qualification and certification practices for AM products [5,6]. They cannot fully replace post-process metrology systems, but they aid anticipated anomaly detection as well as enriched information about part quality. The present study aims to contribute to this specific framework.

Amid the wide literature devoted to in-situ sensing and monitoring in AM [7-9], various studies investigated the possibility of in-situ inspection of dimensional and geometrical deviation, by measuring the deviations from the target geometry observed layerwise [10-15]. These methods rely on the in-situ reconstruction of the printed shape in every layer by means of so-called powder bed cameras commonly available in most industrial powder bed fusion (PBF) systems. The methods proposed in the literature entail a segmentation of high-spatial resolution images of the solidified surface acquired at the end of the melting phase in each manufactured layer. Pagani et al. [14] also proposed to combine the layerwise comparison between the reconstructed shape and the nominal one with a statistical monitoring scheme to automatically signal an alarm in the presence of actual anomalies. However, only few authors investigated the application of layerwise geometry reconstruction to in-situ inspection of lattice structures. Starting from the seminal work by Colosimo et al. [16], proposing an innovative solution for layerwise inspection of lattice structures starting from ex-situ X-ray CT data, Colosimo et al. [17] proposed a novel procedure for in situ inspection of lattice structures via machine learning applied to in-situ images. A similar procedure was proposed in Guerra et al. [18]. Forien et al. [19] proposed a different sensing approach, namely co-axial pyrometry, to detect missing strut errors.

The present study extends and further develops the seminal concept proposed in Colosimo et al. [17], grounding on the seminal idea of modelling in-situ reconstructed quantities and their deviation from the nominal at the unit cell level, what we will call the "*feature" level,* differently from all other works on in-situ monitoring that focused on the deviation at single *layer level.* The proposed methodology involves two major novelty aspects. First, we explicitly address the natural variability affecting in-situ reconstructed geometries gathered via powder bed imaging. Indeed, layer-by-layer varying patterns in the brightness and contrast between the image foreground (i.e., the solidified region) and the background (i.e., the surrounding powder) may result in layer-by-layer varying reconstruction inaccuracies. This inflates the variability of shape deviation metrics and possibly decreases the capability to detect local geometrical distortions. We tackle this challenge through a weighted functional data modelling [20] approach, which allows enhancing the accuracy of the in-line geometry reconstruction, while reducing the prediction error with respect to the ground truth. The second novelty contribution consists of an automated inspection approach where the uncertainty of the in-situ reconstruction is used to design the control limits that can be applied to detect deviations from the nominal geometry while considering the reconstruction error to avoid false alarms. Any deviation violating these limits represents a possible anomaly affecting the way in which the corresponding unit cell is being produced, thus anticipating possible non-conformities in the printed part.

The proposed approach is demonstrated by means of an experimental study involving the production of metal lattice structures with an industrial laser powder bed fusion (L-PBF) system. In-situ sensing was performed using the powder bed camera and lighting setup available in the industrial machine. Ex-situ X-ray CT inspection was used to determine the ground truth of as-built lattice structure geometries. The results highlight the potential to shift the quality inspection of lattice structures from costly post-process controls to cost-effective in-situ and in-line implementation.

The paper is organized as follows. Section 2 presents the proposed methodology. Section 3 presents the real case study, namely the L-PBF production of trabecular lattice structures. Section 4 is devoted to the discussion of results and Section 5 concludes the paper.

2. Methods and materials

2.1. Underlying principle and terminology

The term "lattice structure" refers to a variety of geometrical configurations, ranging from surface-based structures, also known as gyroids, to strut-based structures. The former consists of alternating and intersecting surfaces that repeat in space. The latter consists of a series of rod-like shapes that are connected to each other in different orientations to form unit cells. In this study, we focus on lattice structures characterized by unit cells of fixed size and shape that periodically repeat in space. Thanks to their isotropic characteristics they represent the most common type of structures studied in the literature, which have a wide range of industrial applications.

Regardless of the specific shape and nature of the cells composing the lattice, its structure can be represented in terms of an array of $I \times J \times H$ unit cells of fixed shape and size, placed side by side in a regular grid along the x and y directions, and stacked on top of one another along the z direction, where z also indicates the build direction (Fig. 1). Let l be the side length of the bounding box of each unit cell. Without loss of generally, we consider a cubic bounding box whose volume is equal to l^3 for all cells, as shown in Fig. 1[1]. Being t the layer thickness applied to additively manufacture the lattice structure, then each unit cell consists of $N = l/t$ layers, if both l and t are expressed in mm.

Unit cells can be identified by a unique index i, such that $i = 1,\ldots,I \times J \times H$, such that the spatial location of the i^{th} cell within one copy of the

[1] A possible extension of the methodology to different configurations of lattice structures represents on-going research and future development of the present study.

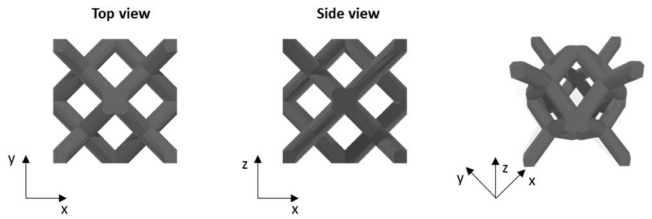

Fig. 2. Top view (left), side view (center) and 3D view (right) of the rhombic unit cell.

Table 1
L-PBF process parameters.

Scan strategy	Scan mode	Laser power	Laser speed	Hatch distance	Layer thickness
Meander	Continuous mode	275 W	1200 mm/s	0.09 mm	0.05 mm

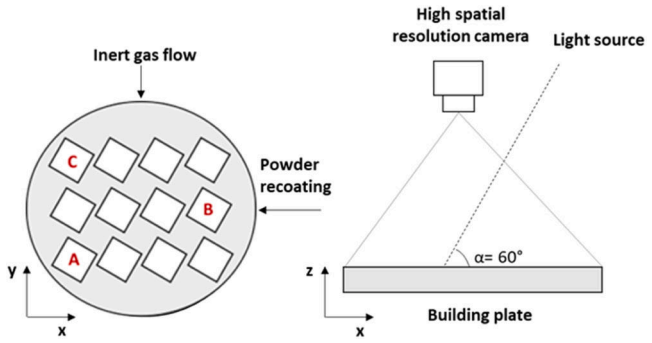

Fig. 3. Specimen location inside the build area (left) and front view of the camera and lighting setup (right).

lattice structure is the same for every other manufactured copy of the same structure. Unit cells can also be identified by the level, h, along the build direction, such that $h = 1,\ldots,H$. Cells placed at the same h^{th} level are manufactured at the same time.

In this paper, the term "nominal shape" refers to the original STL (Standard Triangulation Language) model designed to manufacture the part. The AM production entails a slicing of the nominal 3-D shape into 2-D nominal slices, which can be used as a reference of the desired geometry in every layer. The term "ground truth shape" refers to the as-built manufactured geometry inspected after the process and by means of ex-situ metrology. In this study, we refer to post-process X-ray CT for the ground truth determination. The term "in-situ reconstructed shape" refers to the shape measured via in-situ imaging of every solidified layer.

The proposed approach was tested on a dataset acquired during the production of lattice structures via L-PBF on an industrial Trumpf TruPrint 3000 system. Lattice structures were produced using a gas atomized maraging steel powder. Each lattice specimen was composed of 64 equal rhombic cells, with a struct diameter equal to 1.5 mm. The overall specimen dimension was 40 × 40 × 40 mm, with cell size $l = 10$ mm. Lattice structures were produced with two lateral walls of thickness equal to 0.6 mm, removed from the analysis of the current work. Fig. 2 shows three views of the rhombic unit cell.

Table 1 summarizes the main process parameters adopted to produce the specimens.

The scan direction was rotated by 67° every layer, according to the standard practice in L-PBF. The Trumpf TruPrint 3000 machine was equipped with a Basler acA3800–14uc USB 3.0 camera having a 100μm/pixel spatial resolution and with a light source inclined at about 60° with respect to the building plate. Fig. 3 shows the light source position and the specimen location within the building plate. In the following, results are shown for three copies of the lattice structure named as specimen A, specimen B and specimen C, placed as shown in Fig. 3 (left panel) within the build platform. Two specimens, namely A and B, were used for the calibration phase, while specimen C was used to demonstrate the proposed methodology in the use phase, for in-situ inspection.

As-built specimens were inspected using a North Star Imaging X25 X-ray CT scan system with a voxel size of 33 μm. The registration of the X-ray CT data with respect to the nominal shape followed the same approach proposed in Colosimo et al. [16], based on the Iterative Closest Point (ICP) algorithm.

3. Proposed approach

The overall scheme of the method is shown in Fig. 4. Post-scan powder bed images are acquired in every layer by means of an off-axis powder bed camera. The geometry of the solidified layer is then reconstructed via image segmentation, and dimensional / geometrical properties are estimated for each unit cell on a layer-by-layer basis. One key aspect of the proposed approach consists of moving from a layerwise estimation of any quantity of interest (e.g., the area of the solidified layer within each unit cell) to a 1-D representation of that quantity as a function of the build direction (i.e., step (5) in Fig. 4). In the following, the term "1-D profile" will be used. It refers to the discrete vector of values of the quantity measured in-situ, one value per layer, graphically represented as a discrete curve.

Such 1-D representation can be used as a synthetic "signature" of the dimensional or geometric properties of each manufactured cell, enabling the use of a family of statistical methods known as "profile monitoring" [21-25] for automated detection of local anomalies affecting one or more cells. The term "profile" comes from such class of methods suitable to deal with data patterns in the form of curves.

However, the layer-by-layer variability of in-situ geometry reconstructions is affected by several nuisance factors ([10-13], zur Jacobsmuhlen et al., 2019, [14]). A foremost source of undesired variations involves the chamber lighting setup and the way in which the solidified layer reflects the light towards the camera ([26,11,27]). Being fixed the lighting setup, foreground pixel intensity patterns strongly depend on the solidified surface topography, which in turns is affected by the layerwise varying scan path and direction. This inflates the variability of the image segmentation outcome, reducing the in-situ reconstruction accuracy. Because of this, we present a weighted modelling scheme suitable to enhance the accuracy of the 1-D profile reconstruction, which is on key aspect of the proposed approach.

Leveraging the 1-D profile representation of every manufactured unit cell in the lattice structure, the proposed approach for in-situ automated inspection and detection of possible anomalies consists of two phases. A calibration phase is used to compare the in-situ reconstruction against a reference ground truth (i.e., post-process X-ray CT of the as-built structures). A 1-D profile of the deviation from the ground truth is estimated for all unit cells of M copies of the same structure. The standard error of this deviation is estimated too and used as a measure of the natural variability of the in-situ reconstruction. This standard error allows one to design control limits to be adopted during the actual use phase, i.e., the in-situ inspection of every manufactured structure. While new parts are produced, the 1-D deviation between the in-situ reconstruction and the nominal is computed. If the deviation is within the previously estimated control limits, it is judged to be generated by the natural variability induced by the process and by the in-situ measurement system. If, on the contrary, the 1-D deviation from the nominal is partially or entirely outside these limits, an automated alarm can be signaled, as it points out an anomalous shift whose amplitude cannot be explained purely by the known natural variability.

The details of the methodology are deepened and discussed in the following sub-sections.

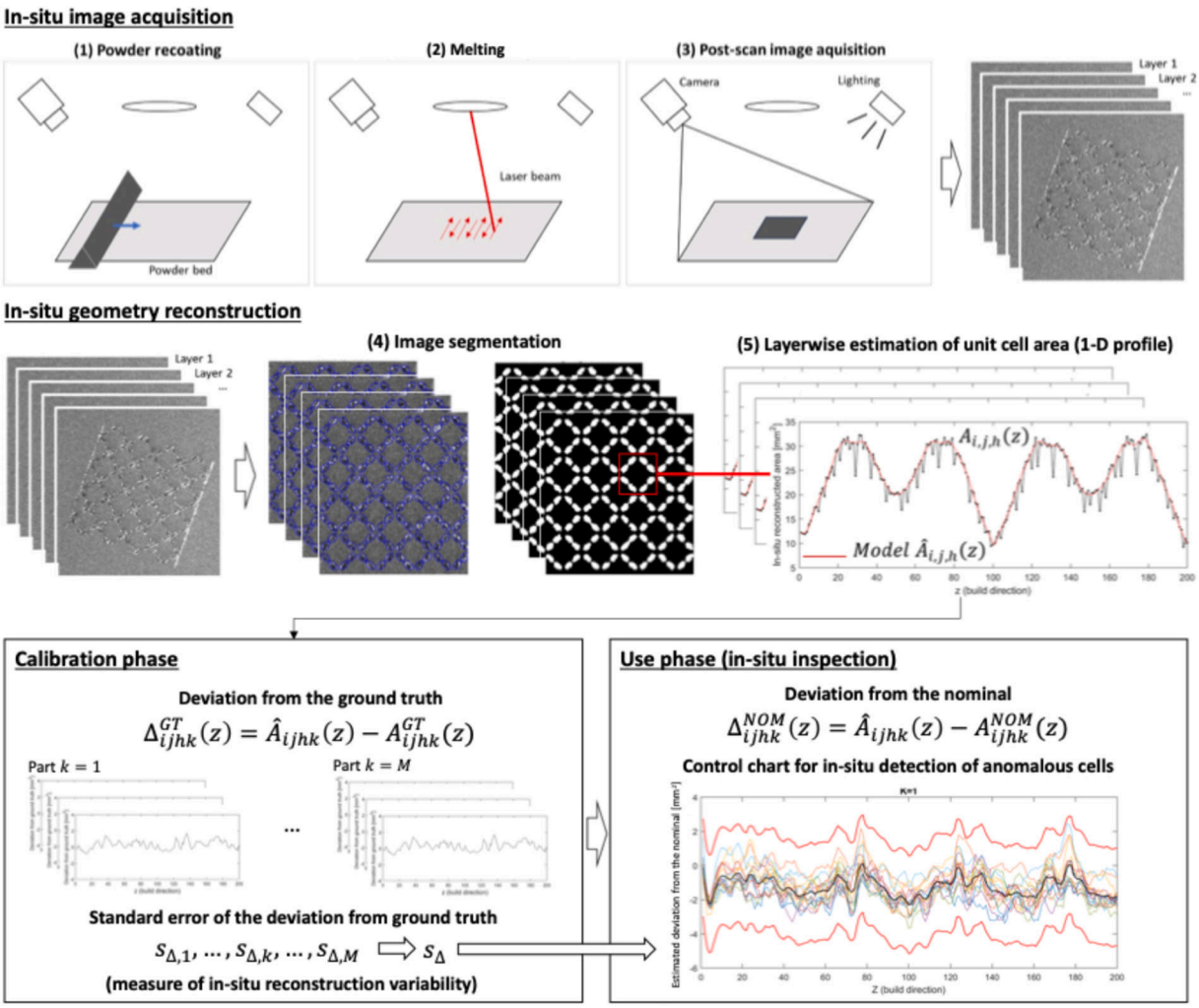

Fig. 4. Scheme of the proposed approach.

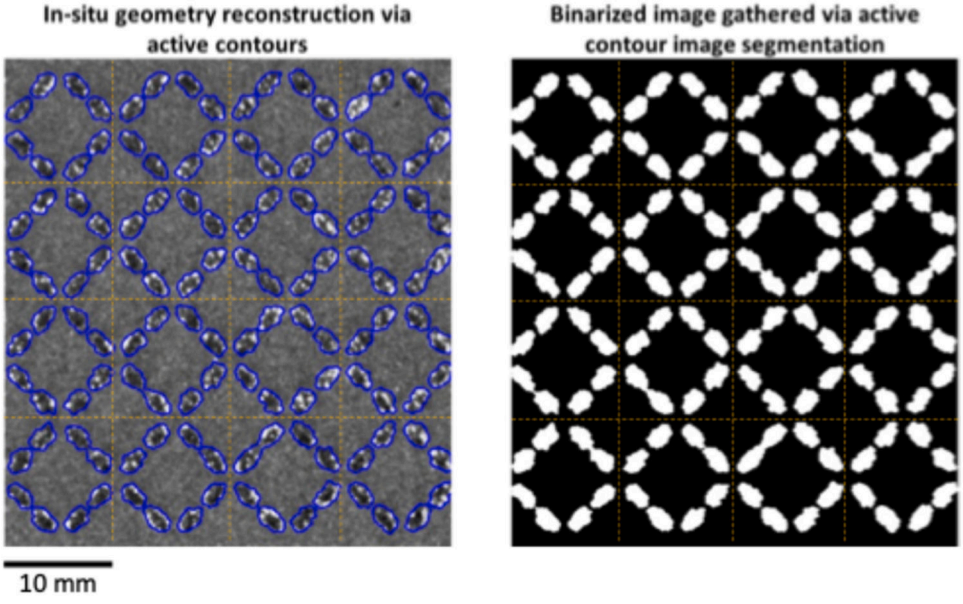

Fig. 5. Example of in-situ determination of the contours of the solidified layer (left panel) and corresponding binary image generation (right panel); vertical and horizontal dashed lines separate individual unit cells.

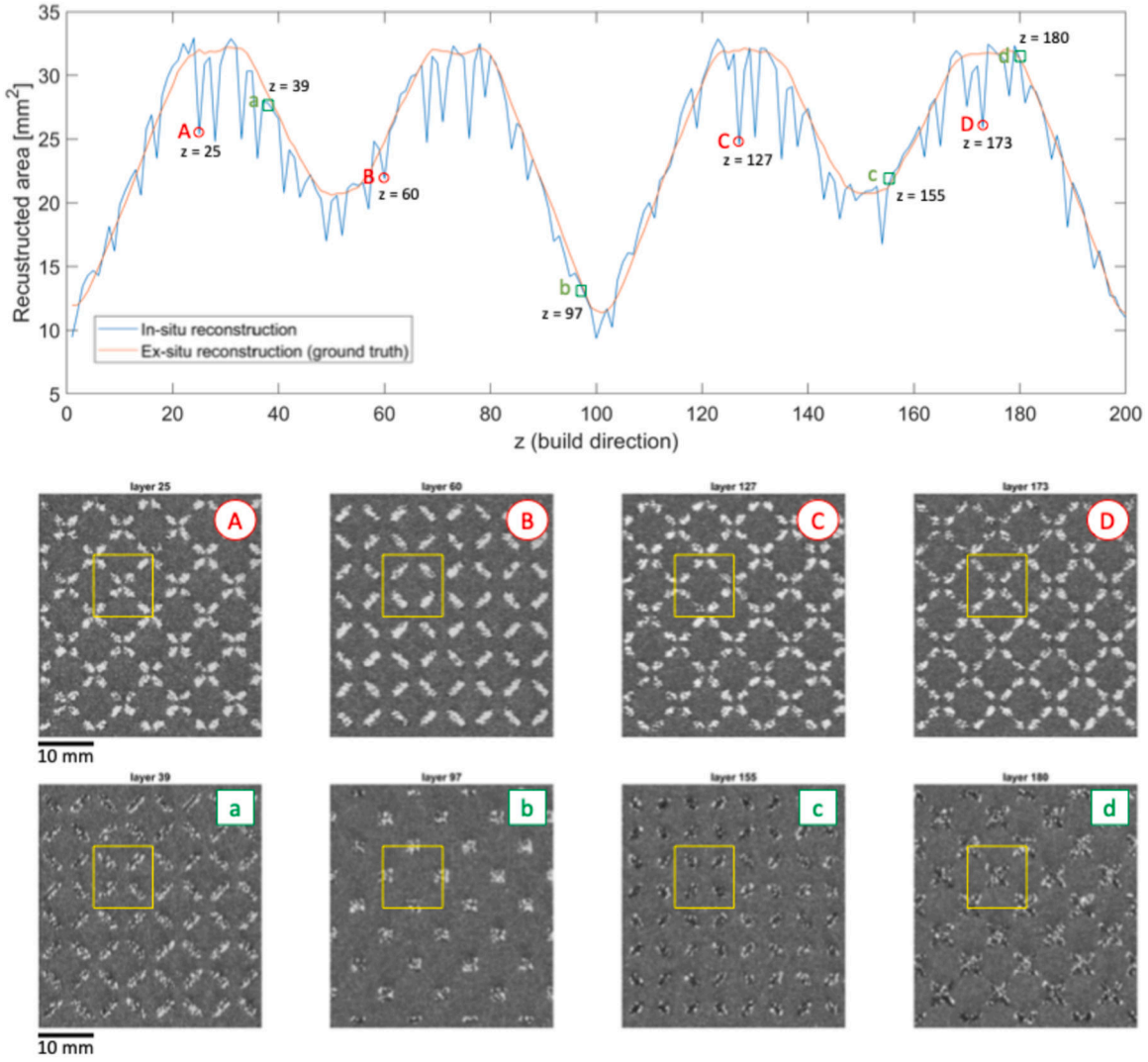

Fig. 6. Top panel: superimposition of in-situ and ex-situ (ground truth) reconstructed area profiles for one cell of specimen A, with periodic fluctuations due to the layerwise 67° scan rotation (see Section 3 for details about the experimental settings); bottom panel: examples of powder bed images in layers where a severe area underestimation with respect to the ground truth was observed (denoted as A, B, C, D) and powder bed images of layers where a good agreement between in-situ and ex-situ reconstructed areas was observed (denoted as a, b, c, d); the ROI of the considered unit cell is highlighted with a square on all powder bed images.

3.1. *In-situ geometry reconstruction*

The in-situ geometry reconstruction relies on a pre-processing step devoted to the perspective correction of the powder bed image and the alignment with respect to the reference geometry (namely the ground truth geometry in the calibration phase, and the nominal geometry in the use phase). Then, powder bed image segmentation is applied for the identification of solidified layer's contours.

Perspective correction and image alignment represent well consolidated methods in image processing, and hence they are not discussed in detail here. The reader is referred to Szeliski [28] and Avants et al. [29] for an overview of available methods. In this study, a standard landmark-based projective algorithm was used for fine alignment between powder bed images and a reference mask [28].

Regarding the in-situ reconstruction of the solidified layer, an active contours methodology is proposed [30,31]. It involves an iterative segmentation that, starting from a first boundary definition in the form of one (or more) closed curve, iteratively changes and adapts the shape of the reconstructed boundary by applying shrink/expansion operations driven by the minimization of an energy functional through the level set formulation [32]. Active contours are particularly suitable to deal with powder bed images in L-PBF, since the nominal geometry of the slice can be used as starting boundary [26,11,33,14]. In this study, we used the method proposed in Pagani et al. [14], which relies on an active contours formulation that combines edge-based and region-based segmentation operations, using the nominal shape as the starting point. Additional details about the methodology can be found in Appendix A.

The output of the segmentation consists of a binarized image, where the original greyscale intensity of the pixels is transformed into a binary set [0,1], as shown in Fig. 5.

3.2. *From layerwise to feature-level modelling*

A key aspect of the proposed approach consists of modelling any dimension and geometrical quantity of interest at unit cell-level, i.e., passing from a layerwise estimate of the quantity to a 1-D curve (or profile) along the build direction, z. This allows estimating a 1-D profile of the deviation from the nominal geometry computed for each unit cell, aiding the detection of local distortions and geometrical errors. In this study we refer to the in-situ reconstructed area of the i^{th} unit cell, $A_i(z)$, as the quantity of interest, but the methodology can be extended and generalized to other quantities as well.

One major challenge to face at this stage regards the layer-to-layer

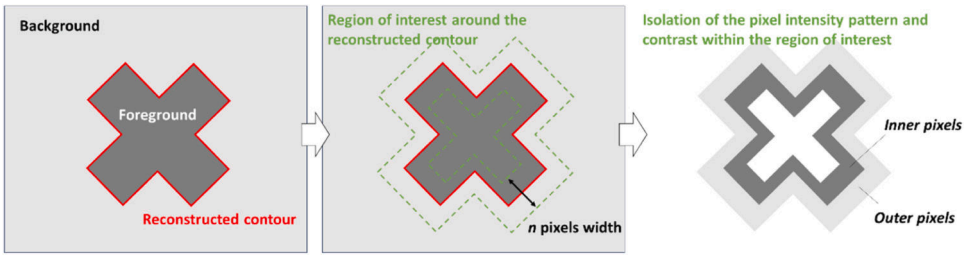

Fig. 7. Example of automated isolation of a region of interest consisting of a band centered along the reconstructed contour to evaluate the pixel intensity contrast between foreground and background.

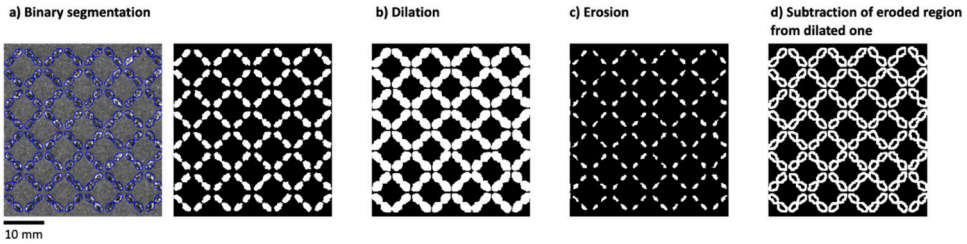

Fig. 8. Morphological operations applied to the binary image obtained as output from the segmentation step; the binary image in panel d) is the band region used for the computation of the weight $\omega(z)$.

variations that affect the 1-D profile, $A_i(z)$. Such undesired variations are largely induced by the chamber lighting setup and the way in which the solidified layer reflects the light towards the camera, which depends also on the layerwise varying scan path and direction. An example of the extent to which such variations may influence the reconstruction accuracy is shown in Fig. 6.

Fig. 6 (top panel) shows an example of the in-situ reconstructed area profile, $A_i(z)$, and the ex-situ reconstructed area profile, hereafter referred to as $A_i^{GT}(z)$, for a unit cell of a lattice structure among the ones discussed in Section 2. The ground truth profile, $A_i^{GT}(z)$, was determined by 1) slicing the X-ray CT reconstruction of the as-built shape, such that every slice corresponds to one printed layer, and 2) applying the same active contours approach to determine the boundaries of the solid material. A fine landmark-based alignment was applied to superimpose the in-situ reconstructed shape with the ground truth mask in every layer.

Despite the two curves in Fig. 6 (top panel) exhibit a good agreement in the underlying pattern, the $A_i(z)$ profile has periodic valleys that deviate from the ground truth leading to an underestimation of the in-situ reconstructed area. Such periodic pattern is driven by the 67° scan rotation applied every layer, which causes a variation of the surface reflections towards the camera and, consequently, a variation of the in-situ area estimation. Fig. 6 (top panel) also shows that the peaks of the $A_i(z)$ profile oscillate above and below the ground truth area profile, which indicates the absence of a systematic bias in layers where favorable light reflection conditions are met.

The valleys shown in Fig. 6 (top panel) correspond to layers where the scan direction produced a bright-field-like intensity pattern, and hence a worse reconstruction of the solidified geometry. Fig. 6 (bottom panel) highlights four examples of powder bed images corresponding to four such valleys, labeled with capital letters, together with four examples of powder bed images corresponding to layers were there was a very good agreement between in-situ and ex-situ reconstructed areas, labeled with lowercase letters. The examples in Fig. 6 (bottom panel) show that layers where a large deviation from the ground truth was observed also exhibited a more intense light reflection, visible as a higher pixel intensity within the whole solidified region. This occurred at specific scan directions with respect to the fixed camera orientation, being the scan angle varied by 67° every layer as in the common industrial practice. Notably, also the amplitude of the valleys depends on the intensity pattern observed at each layer too, and is not constant, thus inducing an additional level of variability.

A high intensity of foreground pixels is typical of so-called "bright field" illumination conditions, which are known to yield poor edge detection results, as they tend to force the segmentation algorithm to isolate the brightest area rather than the real boundary between foreground and background regions [34].

This undesired variability of in-situ reconstructed dimensional and geometrical properties of the part can be tackled and mitigated in three possible ways. One would consist of finding a powder bed image segmentation algorithm that is insensitive to layerwise varying pixel intensity patterns and contrasts. However, although margins for improvements exist, tuning or changing the algorithm would be hardly sufficient to fix the problem, as the segmentation performances necessarily depend on the information enclosed in the image. Another solution would consist of rethinking the way in which powder bed images are acquired, minimizing, or even avoiding, layerwise variations of captured patterns. This is an interesting and promising research direction (which also represents an on-going research and future development of the present study), but it would imply using a sensing equipment different from those currently available in every L-PBF system. Examples can be found in Bugatti and Colosimo [35], and Tan Phuc and Seita [36]. The third solution consists of designing a profile modelling approach that explicitly considers the intrinsic variations of in-situ shape reconstructions, aiming to reduce the variability of in-situ quality estimates and enable a more accurate assessment of departures from the nominal geometry. This third research direction is the one addressed by the present study.

The underlying principle consists of fitting a weighted model to the 1-D profile of the quantity of interest such that a lower weight is given to layers where pixel intensities and contrast patterns are likely to generate a low contour reconstruction accuracy, while a high weight is given to all other layers. To this aim, we propose a weighting scheme whose rationale is schematically shown with the aid of Fig. 7.

In the presence of intense light reflections or even saturated pixels within the solidified region, a large variation is expected between foreground and background pixel intensities. Thus, the inverse of this variance can be used as a weight in the fitted model. We propose to estimate the weight by automatically identifying a ROI that is centered on the in-situ reconstructed contour in every layer. The ROI is such that

its inner portion includes foreground pixels, while the outer portion includes background pixels. Fig. 8 schematically shows one automated way to isolate, on a layer-by-layer basis, the ROI in the form of a band of width equal to n pixels. Let $b(z)$ be the band region identified in the z^{th} layer and let ${s_b}^2(z)$ be the pixel intensity variance of all pixels belonging to the $b(z)$. Then, the proposed weight $\omega(z)$ function is proportional to the inverse of ${s_b}^2(z)$:

$$\omega(z) = \frac{1}{{s_b}^2(z)} \tag{1}$$

A larger value of $\omega(z)$ implies a higher confidence in the accuracy of the in-situ reconstruction, whereas a lower value implies a lower confidence.

The proposed approach to identify the band region and to estimate the weight $\omega(z)$ in each layer relies on a combination of image processing operations known as morphological dilation and erosion operations. Such operations are applied to the binary image generated by the active contours algorithm. The erosion operation shrinks the boundary of the reconstructed contour towards the inside, whereas the dilation expands it towards the outside. They result from the application of a square structuring element of size $n \times n$ pixels such that if at least one pixel in the structuring element coincides with a foreground pixel, then all pixels are labelled as foreground if dilation is applied, and the opposite if erosion is applied. A real example of these two operations is shown in Fig. 8. The ROI is finally obtained by subtracting the eroded image from the dilated one, resulting in a band region centered along the in-situ reconstructed contour (Fig. 8, panel d).

The weight $\omega(z)$ is then used to fit a weighted least square (WLS) model to the 1-D profile of the in-situ reconstructed quantity, i.e., $A_i(z)$. We advocate the combination of a weighted least-squares scheme with a B-Spline functional model [37]. A B-Spline model of $A_i(z)$ is denoted as $\widehat{A}_i(z)$, and it can be defined as:

$$\widehat{A}_i(z) = \sum_{q=1}^{Q+L-1} B_q(z,\tau) P_{i,q} \tag{2}$$

$$i = I \times J \times H, \quad z = 1, \ldots, N$$

where B_q are the B-Spline basis functions, defined using the Cox-de Boor algorithm, of order $Q = 3$. The basis functions depend on the choice of the knot sequence, $\boldsymbol{\tau} = \{\tau_l, l = 1, 2, \ldots, L-1\}$ where L is the number of subintervals. $P_{i,1}, P_{i,2}, \ldots, P_{i,Q+L-1}$ are the control points for the i^{th} unit cell. They can be computed using the WLS method as follows:

$$P_i = \left(B^T W(z) B\right)^{-1} B^T W(z) A_i(z) \tag{3}$$

where B is the model matrix with the B-splines basis functions and $W(z)$ is a diagonal matrix whose diagonal elements are the weights $\omega(z)$ multiplied by a corrective factor $S = \sum_{z=1}^{N} \frac{1}{{s_b}^2(z)}$.

The number of knots and their location within the vector $\boldsymbol{\tau}$ can be estimated in the calibration phase. Another parameter to be defined is the width of the band region, n, expressed in number of pixels. n shall be an odd number, as the centroid of the squared element of size $n \times n$ pixels used for erosion and dilation operations belongs to the contour, and the band extends n^* pixels towards the foreground region and n^* pixels towards the background. Therefore, $n = 1 + 2n^*$. The width n should be selected such than n^* is lower than half the minimum width of the foreground region, and greater than at least 2 or 3 pixels to avoid too narrow bands. In this study, we used $n = 11$, which corresponds to 1.1 mm.

Eventually, it is worth noticing that by assigning a low weight to layers where the pixel intensity pattern is expected to cause a poor reconstruction accuracy, actual geometrical anomalies affecting only those layers may be mitigated as well. However, if the deviation from the nominal shape occurs is consistently occurring in consecutive layers, the proposed approach is suited to detect it while reducing possible false alarms due to reconstruction inaccuracies affecting individual layers with no effect on the final part quality.

3.3. In-situ inspection and automated detection of local anomalies

The proposed methodology is aimed at detecting, in-situ and in-process, any actual distortion and geometrical error affecting one or multiple unit cells of manufactured lattice structures. The underlying principle consists of monitoring the deviation between the in-situ reconstructed profile, $\widehat{A}_i(z)$, and the nominal one, hereafter referred to as $A_i^{NOM}(z)$, while considering the natural variability of the in-situ reconstruction. To this aim, the method entails two sequential phases, namely a calibration phase and the actual use phase. They are described in the following two sub-sections.

3.3.1. Calibration phase

The aim of the calibration phase is to determine the standard error of the in-situ reconstruction with respect to a ground truth reference. It is then used as a measure of the in-situ reconstruction variability to design the control limits that are applied during the inspection of every manufactured part during the following use phase.

As a ground truth we refer to the X-ray-CT measurement of the as-built structure. The X-ray CT reconstruction can be sliced along the build direction such that successive slices are spaced apart by a distance equal to the layer thickness. The active contour segmentation can be applied to the X-ray CT slices and the result can be aligned, on a slice-by-slice basis, to the in-situ reconstructed geometry. Let M be the number of copies of the same lattice structures that are made available during the calibration phase. Then, the deviation between the in-situ reconstruction and the ground truth can be expressed as follows:

$$\Delta_{i,k}^{GT}(z) = \widehat{A}_{i,k}(z) - A_{i,k}^{GT}(z) \quad , \quad k = 1, \ldots, M \tag{4}$$

During the calibration phase, the parameters of the in-situ segmentation based on the active contours algorithm can be tuned to minimize the deviation from the ground truth, $\Delta_{i,k}^{GT}(z)$. Once the optimal in-situ reconstruction settings have been determined, the standard error of the deviation from the ground truth is estimated for each copy of the lattice structure, as the average standard error of all unit cells belonging to the structure, namely $s_{\Delta,1}, \ldots, s_{\Delta,k}, \ldots, s_{\Delta,M}$. The overall pooled standard deviation, s_Δ, namely the average of individual standard deviations, is then used as a measure of the natural variability of the deviation. Such variability measurement allows one setting control limits to be applied in the use phase.

3.3.2. Use phase

The use phase consists of the actual in-situ inspection operation, conceived to enable the automated detection of undesired variations of the dimensions and shape of individual unit cells during the AM process. Differently from the calibration phase, the reference to determine the quality of the build is the nominal area, $A_i^{NOM}(z)$, as the deviation from the nominal is the only type of deviation that could be assessed while the part is being built:

$$\Delta_{i,k}^{NOM}(z) = \widehat{A}_{i,k}(z) - A_{i,k}^{NOM}(z) \quad , \quad k = 1, 2, \ldots \tag{5}$$

We propose a control charting scheme for automated anomaly detection with control limits in the form:

$$\overline{\Delta_h^{NOM}}(z) \pm k s_\Delta \tag{6}$$

where $\overline{\Delta_h^{NOM}}(z)$ is the sample mean deviation across all unit cells built up from height level $h = 1$ to the current height level h, whereas $k = z_{\alpha/2}$ is the upper $100\left(\frac{\alpha}{2}\right)\%$ percentile of the standard normal distribution, and α is the family-wise false positive error, also known as Type I error.

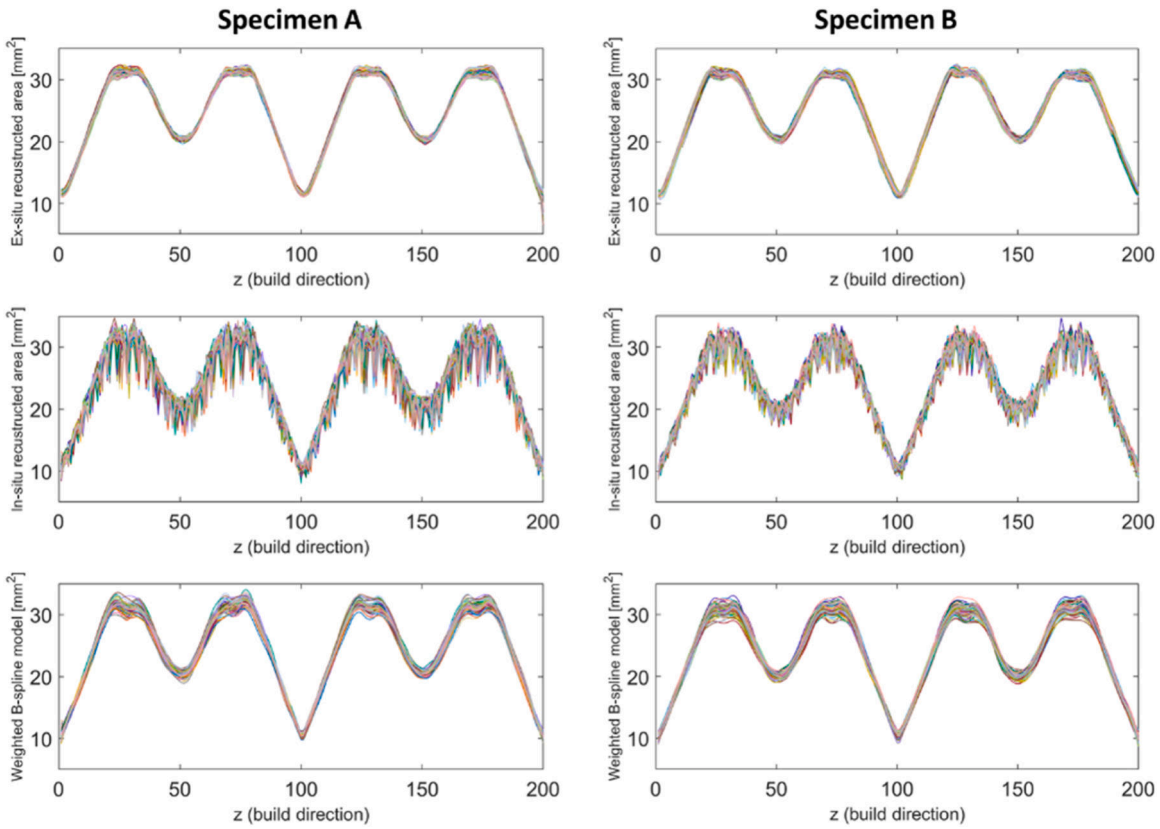

Fig. 9. Comparison of ex-situ (top panel) and in-situ (central panel) reconstructed area profiles for all the unit cells of the three specimens, while bottom panels show the proposed weighted B-Spline models of in-situ reconstructed area profiles, $\widehat{A}_i(z)$.

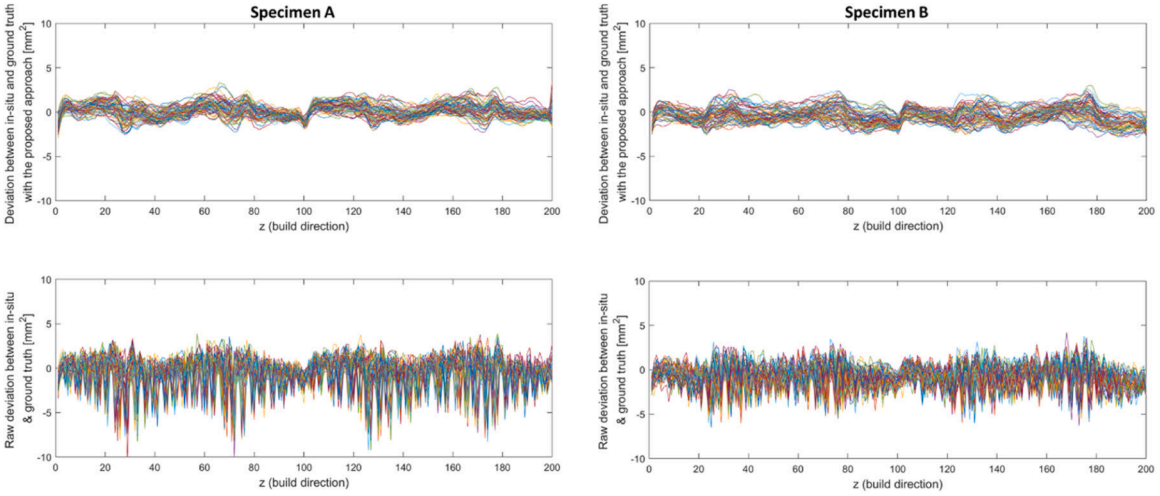

Fig. 10. deviation profiles $\Delta_i^{GT}(z)$ for all the unit cells of the calibration specimens (top panels), and the corresponding raw deviation $\Delta_i^{GTraw}(z)$.

Being l the number of layers within one unit cell, i.e., the number of datapoints along the $\Delta_i^{NOM}(z)$ profile, the familywise α error can be determined as $\alpha = \alpha^*/l$, where α^* is the target Type I error. In this study, we used $\alpha^* = 0.0027$, as in the common statistical process monitoring practice.

Since unit cells are built on top of each other, once all the cells at the height level h have been manufactured, their corresponding deviation profiles, $\Delta_i^{NOM}(z)$, can be estimated, the sample mean $\overline{\Delta_h^{NOM}}(z)$ can be computed, and the individual deviation profiles can be compared against the control limits in Eq. (6).

Setting the control limits at $\pm k$ times the standard deviation estimated during the calibration phase, i.e., s_Δ, allows tuning the control limit design based on the natural variation from the ground truth reference. The more accurate is the in-situ reconstruction, the smaller is s_Δ, and the tighter control limits could be, thus enabling an enhanced detectability of small deviations.

It is worth noticing that other metrics, different from the one in Eq. (5), can be considered to quantify the deviation from the nominal shape. Examples have been proposed in Pagani et al. (2021) and Colosimo et al. (2022). Each metric has its own advantages and limitations. The area-based deviation in Eq. (5) is robust to small misalignment errors

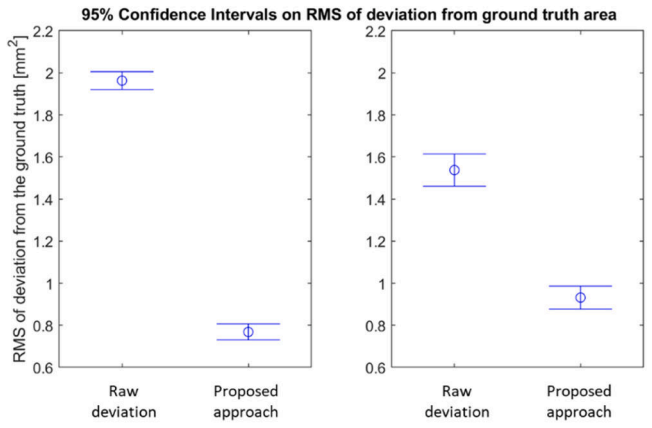

Fig. 11. 95 % confidence intervals of the RMS of the deviation from the ground truth for the raw deviation $\Delta_i^{GTraw}(z)$ and the deviation based on the proposed weighted model $\Delta_i^{GT}(z)$ (left panel: specimen A, right panel: specimen B).

between the powder bed image and the nominal shape, but it is not suitable to detect geometrical errors that do not cause any variation in the solidified area. However, the proposed approach can be applied regardless of the specific deviation metric. A performance analysis including a comparison among different ways to quantify the deviation from the nominal can be part of future investigations.

4. Results

4.1. Calibration

Fig. 9 shows a comparison between 1-D profiles of in-situ reconstructed areas, $A_i(z)$, their weighted B-Spline model, $\widehat{A}_i(z)$, and the corresponding 1-D profiles of ex-situ reconstructed areas, $A_i^{GT}(z)$, for all unit cells of analyzed lattice structures. Fig. 9 shows a superimposition of profiles for all unit cells of specimens A and B.

Fig. 9 (top panels) shows that the "signature" in terms of the printed area of all cells in both analysed structures is highly repeatable. The profile pattern along the build direction depends on the specific geometry of the rhombic cell. Fig. 9 (central panels) shows that the same underlying pattern is captured by the in-situ reconstruction, although periodic valleys inflate the variability of $A_i(z)$ profiles, introducing major deviations from the ground truth. Fig. 9 (central panels) also shows that such valleys are prominent in specimen A, while less evident in specimen B. Indeed, depending on the part location within the build area, layerwise variations caused by the varying scan direction may result in stronger or weaker variations of the light reflected towards the camera, with a consequent stronger or weaker effect on the image segmentation performance.

Fig. 9 (bottom panels) shows that by fitting the proposed weighted model those local inaccuracies are filtered out, leading to an estimation of the reconstructed area profile, $\widehat{A}_i(z)$, that is much closer and more representative of the actual ground truth. Due to the smoothness of the area profile, we adopted a simple B-Spline knot sequence $\boldsymbol{\tau}$ composed by 21 equi-spaced knots along the z direction to fit the model.

To better highlight the consistency between the in-situ reconstruction and the ground truth reference, Fig. 10 shows the deviation profiles $\Delta_i^{GT}(z)$ for all the unit cells of the calibration specimens (top panels), and the corresponding raw deviation $\Delta_i^{GTraw}(z)$ defined as:

$$\Delta_i^{GTraw}(z) = A_i(z) - A_i^{GT}(z) \tag{7}$$

where the ground truth area is subtracted from the raw area, $A_i(z)$, rather than from the proposed weighted model. Fig. 10 shows that the

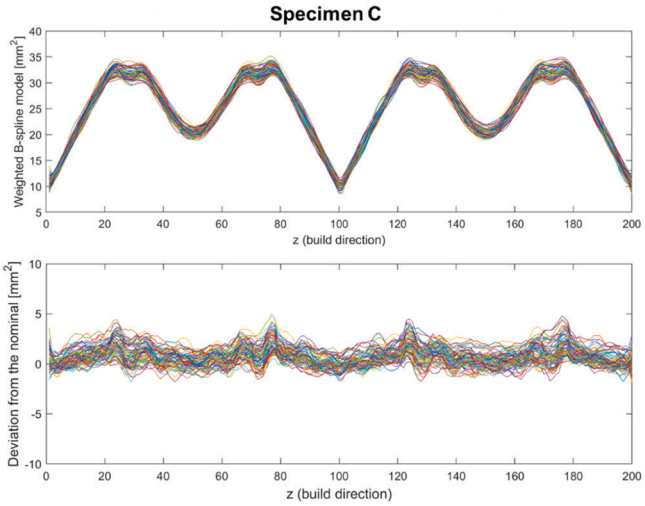

Fig. 13. in-situ reconstructed 1-D area profiles $\widehat{A}_i(z)$ for specimen C (top panel) and the corresponding deviation from the nominal (bottom panel).

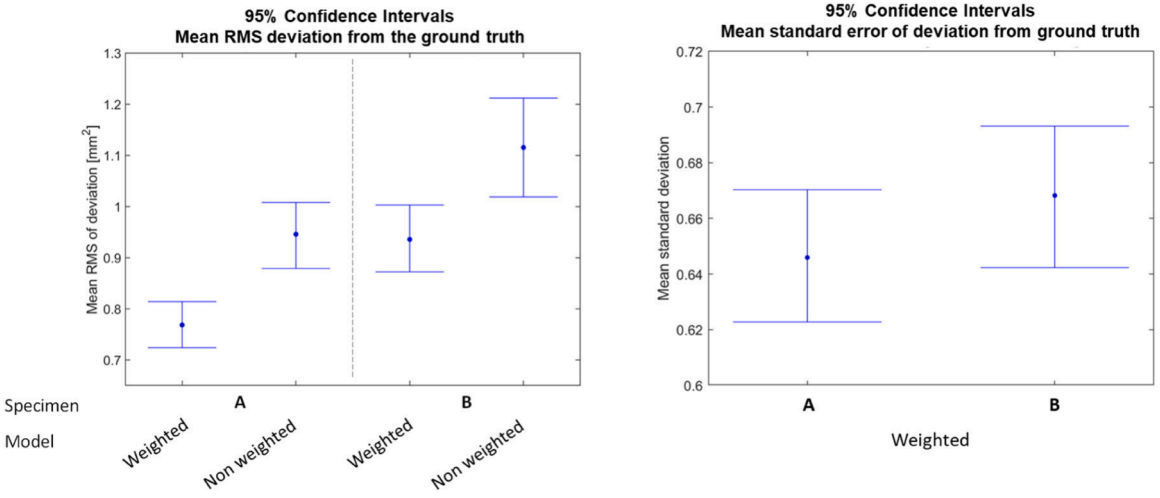

Fig. 12. – 95 % confidence intervals for the mean RMS deviation from the ground truth, comparing the proposed weighted B-spline model against a standard least square (non-weighted) model (left panel); 95 % confidence intervals for the mean standard error of the deviation from the ground truth obtained by using the proposed (weighted) approach (right panel).

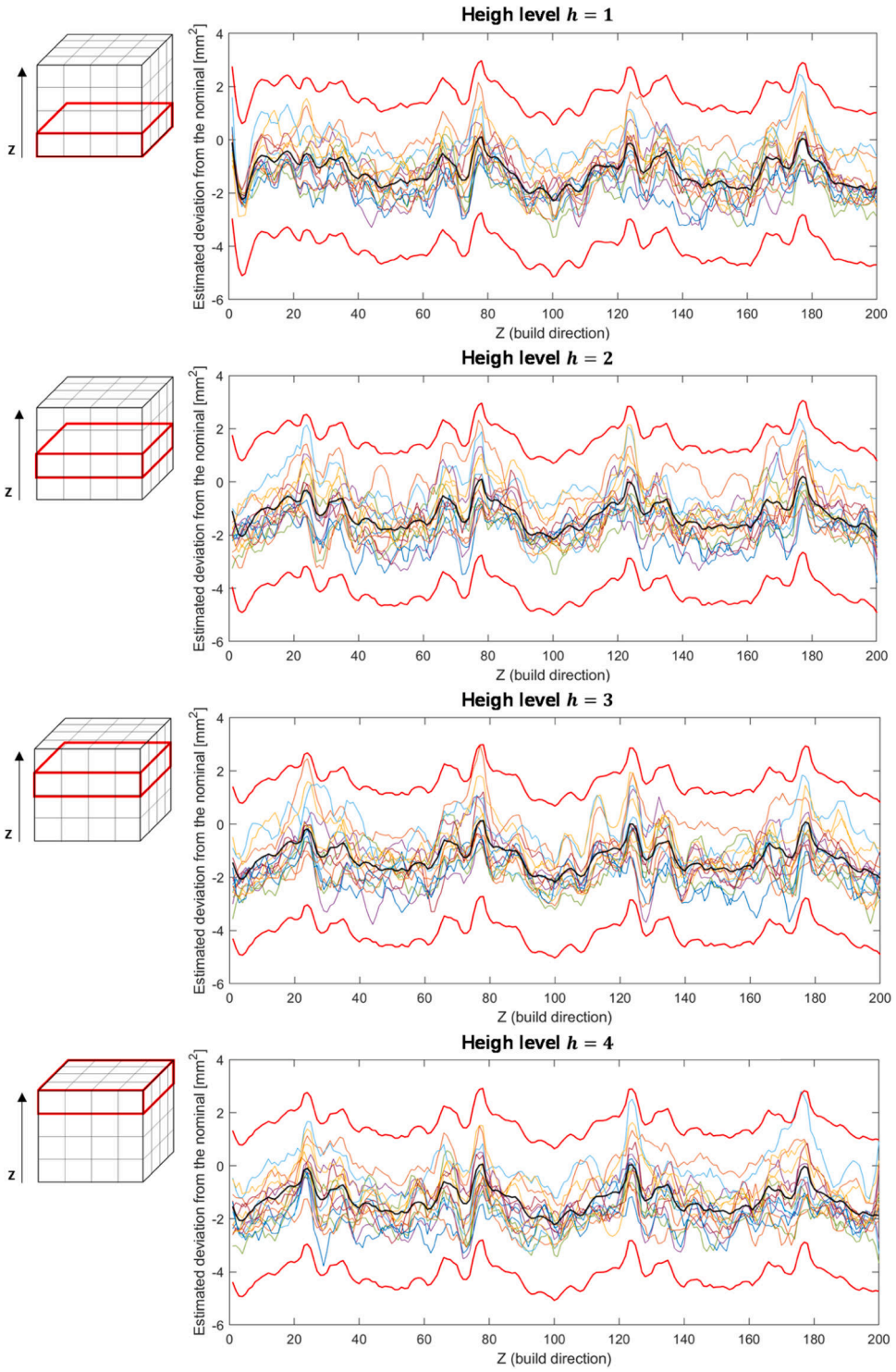

Fig. 14. Control charts for in-situ inspection of specimen C; each panel refers to unit cells produced at a given height level, $h = 1, \ldots, 4$.

proposed weighted modelling approach allows a considerable reduction of the variability of the deviation from the ground truth. $\Delta_i^{GT}(z)$ profiles vary between ± 3 mm^2, which means that the deviation between in-situ and ex-situ reconstructed areas is one order of magnitude lower than the measured area itself.

Fig. 11 shows a quantitative comparison between the root mean square (RMS) of the raw deviation from the ground truth, $\Delta_i^{GTraw}(z)$, and the RMS of the deviation based on the proposed weighted model, $\Delta_i^{GT}(z)$.

Fig. 11 shows that the proposed modelling approach yields a considerable and statistically significant reduction of the mismatch between in-situ estimated areas and the ground truth reference. The improvement is more evident for specimen A, i.e., the one that was more affected by the layerwise variation of the pixel intensity pattern. The resulting RMS of the deviation from the ground truth area is lower than 1 mm^2 for specimens A and B. Such deviation between in-situ and ex-situ reconstructed areas corresponds to an average deviation in terms of average strut thickness lower than 0.1 – 0.2 mm, i.e., in the same order of magnitude of the powder bed image's spatial resolution.

Fig. 12 (left panel) shows a comparison between the proposed

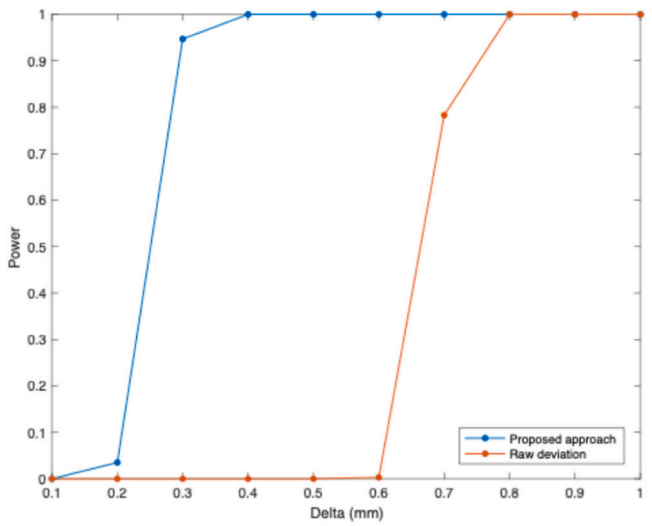

Fig. 15. Power curves for the simulated anomaly consisting of a lack of material affecting the 60^{th} unit cell of Specimen C: comparison between the proposed approach and the competitor approach involving a control chart designed and applied directly to the raw deviation profiles.

weighted model and a model that entails no weighting scheme, i.e., a standard ordinary least square model. The competitor approach simply consists of fitting a B-Spline model of the same order and type, and with the same knot sequence, but without the introduction of the weight matrix W. In practise, this model does not consider the intrinsic variations of the surface reflections periodically occurring because of varying scan directions. Fig. 12 (left panel) shows that, for specimen A and B, the proposed weighted model yields a more accurate reconstruction than using an ordinary least square model.

Fig. 12 (right panel) compares the confidence intervals of the mean standard errors of the deviation from the ground truth, $\Delta_i^{GT}(z)$, estimated using the proposed weighted B-spline model. It shows that there is no statistically significant difference in the natural variations from the ground truth reference between the two specimens. This allows using the pooled standard deviation s_Δ to design the control limits to be used in the actual use phase, namely for in-situ inspection of other manufactured lattice structures.

The consistency of the standard error of the deviation across all individual unit cells of specimens A and B is also displayed in Appendix B, where the 95 % prediction intervals of the deviations from the ground truth are shows for each cell. Figures B1 and B2 in Appendix B highlight that all prediction intervals include the 0, which confirms that the in-situ reconstruction is not statistically different from the ground truth reference in terms of the proposed deviation metric. Moreover, they show that the amplitude of prediction intervals is very similar for all unit cells, which confirms that the natural variability of the reconstruction is stable both within and between calibration samples.

4.2. In-situ inspection

In this study, we referred to the third sample, specimen C, to demonstrate the use of the proposed method for in-situ inspection.

Fig. 13 shows the in-situ reconstructed 1-D area profiles $\widehat{A}_i(z)$ for specimen C and the corresponding deviation from the nominal.

Fig. 13 shows that the 1-D pattern of the in-situ reconstructed area, $\widehat{A}_i(z)$, for specimen C is close to the one observed for the other two specimens. The deviation from the nominal oscillates around 0 with peak deviations in the range $-2 \div 5$ mm^2. The proposed control charting scheme for in-situ quality inspection was applied to such deviations from the nominal shape for unit cells manufactured at increasing height levels above the baseplate. The resulting control charts are shown in Fig. 14.

Fig. 14 shows that all unit cells at all height levels are within the control limits. This highlights the absence of dimensional and geometrical errors, which was confirmed by the post-process inspection of specimen C. Once the production of the h-th level of unit cell is completed, the corresponding control chart can be generated and displayed. In case of any violation of the control limits, an automated alarm can be signaled, and the operator may decide whether any action is needed. As the process goes on, new control charts for subsequent height levels are generated and displayed, enabling the on-line inspection of the whole structure. The same approach can be applied in the presence of multiple lattice structures manufactured in the same build. Ongoing research is devoted to the characterization of the anomaly detection performance of the proposed approach in the presence of real deviations.

4.3. Performance analysis

An additional analysis was performed to determine the power of the proposed control charting scheme for automated detection of anomalous deviations from the nominal. To this aim, a lack of material was simulated by dilating the nominal contour of one unit cell belonging to Specimen C in a subset of layers. By dilating the nominal geometry, the in-situ reconstructed area results to be smaller than the nominal, which is representative of defects that may occur in-process, leading to insufficient solidified material in a given region.

The simulation settings were the following. The anomaly was intruded in the 60^{th} unit cell of Specimen C (placed at level $h = 4$), in

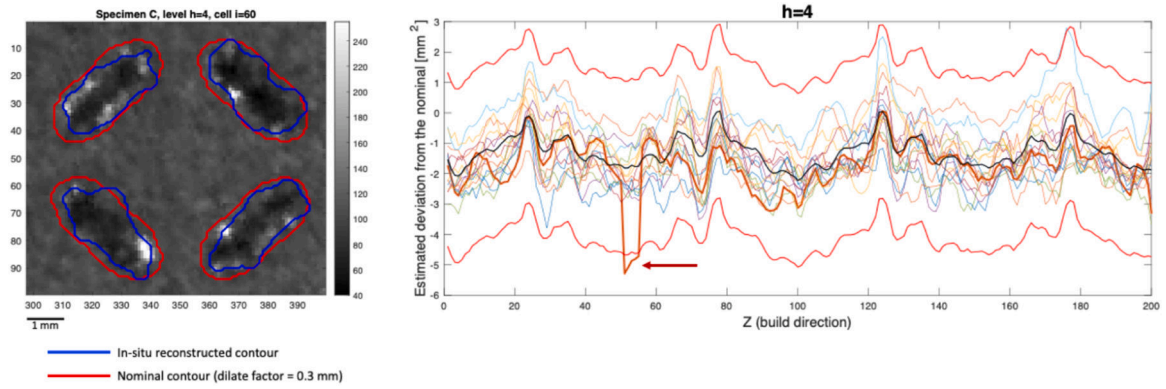

Fig. 16. Left panel: sample image of one layer of the 60^{th} unit cell of Specimen C with a superimposition of both in-situ reconstructed and nominal contours (dilation factor = 0.3 mm); right panel: example of control chart with the injection of the simulated anomaly with dilation factor = 0.3 mm in layer $z = 51$ to $z = 60$ (the detected anomaly is indicated by the arrow).

five consecutive layers, randomly selected. The magnitude of the dilation applied to the nominal geometry was in the range [0,10] pixels, with a step of 1 pixel, corresponding to a deviation of [0,1] mm, given the 100 μm/pixel resolution of the camera. The dilation was randomly applied in different layers, and for each dilation magnitude the power of the control chart was determined as the ratio between the number of detected anomalies and the total number of simulated anomalies. Such analysis was performed for the proposed approach, relying on the weighted least square fitting of the deviation profiles, and for a competitor approach where the raw deviation profiles are used without any fitting. Such competitor approach is representative of performances that could be achieved by directly comparing the in-situ reconstructed contours with the nominal shape, without any profile modeling step. In both cases, the control limits were estimated using the data gathered for Specimen A and B, and discussed in sub-Section 4.2.

Fig. 15 shows the power curves for the proposed approach and its basic competitor. Fig. 15 shows that the proposed approach allows detecting an anomalous deviation of 0.3 mm (three times the spatial resolution of the camera) with a probability of detection higher than 90 %. For the competitor approach, instead, the probability of detection raises above 90 % only for deviations larger than 0.7 mm. This is due to the much larger variability of the raw deviation profiles compared to their weighted least square estimations. Such larger variability inflates the false negative rates, reducing the power of the control charts.

Fig. 16 (left panel) shows an example of the 60^{th} unit cell in one layer, with a superimposition of both the in-situ reconstructed contours and the nominal ones with dilation factor equal to 0.3 mm. Fig. 16 (right panel) shows an example of control chart for the cells places at level $h = 4$ of Specimen C, where a lack of material was simulated in layer $z = 51$ to $z = 60$. The red arrow indicates the detection of such anomaly.

The results highlight the benefit of modelling the 1-D deviation profiles from the nominal with a weighting scheme aimed at mitigating the extra variability induced by the layerwise varying pixel intensity patterns in powder bed images. Future developments will involve testing the proposed approach in the presence of real defects, to validate its suitability as in-line and in-situ inspection and monitoring tool.

5. Conclusions

Given the increasing shape complexity enabled by the widespread adoption of AM technologies, process and quality engineers must face new challenges related to the design of suitable and efficient product qualification methodologies and statistical quality modelling and monitoring instruments. Lattice structures represent a class of innovative complex shapes that impose to rethink qualification methods and procedures in a more efficient way. Leveraging on high resolution imaging made available by embedded powder bed cameras in L-PBF, we presented a method to support the in-line inspection of periodic lattice structures and the anticipated detection of geometrical distortions while the part is being built. The method aims to model the deviation of the in-situ reconstructed geometry from the nominal one at feature level, i.e., at the level of the unit cell, rather than at layer level. One key issue of the proposed approach is its ability to address the natural variability involved in geometry reconstructions from in-situ powder bed images. The proposed approach, relying on a 1-D functional representation combined with a weighted modelling technique, allows enhancing the accuracy of in-situ reconstructions. The accuracy improvement was demonstrated in a real case study where X-ray CT scan of as-built structures was used as ground truth. Moreover, an automated control chart scheme was presented to enable the automated detection of anomalous deviations from the desired shape. A preliminary analysis highlighted the effectiveness of the approach in detecting such anomalies and its enhanced power with respect to directly monitoring raw deviations between in-situ reconstructed and nominal contours.

The proposed approach opens the possibility to move from expensive and time-consuming ex-situ inspections to in-situ analysis, to detect anomalous dimensional and geometrical errors affecting individual cells in a serial production of lattice structures. A future work will test the proposed approach in the presence of actual geometrical distortions, aiming to demonstrate the suitability of the method to anticipate the detection of real anomalous shifts. The authors are working on two other promising research directions. One regards the transferability of the proposed modelling framework to more complex lattice structures, where unit cells are characterized by dimensional and/or geometrical variations within the structures. One further research direction consists of combining the proposed approach with alternative sensing methods. Although powder bed cameras are easily available in L-PBF systems, they produce images that are prone to a wide variety of nuisance effects and undesired sources of variability. The modelling approach proposed in this paper was specifically aimed at tackling some of these issues, allowing a more effective use of powder bed images from industrial cameras. Another promising way to tackle the problem consist of combining an in-line quality modelling approach, like the one here proposed, with an enhanced sensing setup, where perspective errors, misalignments and layerwise varying effects caused by light reflections are mitigated or even avoided. Examples can be found in Bugatti and Colosimo [35], and Tan Phuc and Seita [36]. Indeed, we believe that the key to bridge the gap between research solutions and industrial applications relies in the ability to merge and combine advanced data modelling methodologies with novel and effective in-situ data acquisition techniques.

CRediT authorship contribution statement

Marco Grasso: Writing – original draft, Validation, Software, Methodology, Data curation, Conceptualization. **Bianca Maria Colosimo:** Writing – review & editing, Writing – original draft, Validation, Supervision, Methodology, Funding acquisition, Conceptualization. **Luca Pagani:** Software, Methodology, Data curation, Conceptualization. **Federica Garghetti:** Writing – original draft, Validation, Software, Data curation.

Declaration of Competing Interest

The authors declare the following financial interests/personal relationships which may be considered as potential competing interests: Bianca Maria Colosimo reports financial support was provided by Polytechnic of Milan Department of Mechanics. If there are other authors, they declare that they have no known competing financial interests or personal relationships that could have appeared to influence the work reported in this paper.

Acknowledgements

This study was carried out within the MICS (Made in Italy – Circular and Sustainable) Extended Partnership and received funding from the European Union Next-GeneraFonEU (PIANO NAZIONALE DI RIPRESA E RESILIENZA (PNRR) – MISSIONE 4 COMPONENTE 2,
INVESTIMENTO 1.3 – D.D. 1551.11–10–2022, PE00000004).

Appendix A

The foreground contour in one layer can be represented as the zero-level set of a signed distance function, $\varphi(x, y)$, defined as follows:

$$\varphi(x,y) = \begin{cases} -d(x,y,\delta\Omega) if (x,y) \in \Omega \\ d(x,y,\delta\Omega) if (x,y) \notin \Omega \end{cases} \quad \text{(A1)}$$

where the region Ω corresponds to the foreground (i.e., the solidified layer), and $d(x,\delta\Omega)$ is the distance between any pixel in the (x,y) location and the boundary $\delta\Omega$ of the region Ω. At the first iteration, namely at $t = 0$, the signed distance $\varphi(x,y,t=0)$ is computed using the nominal shape of the manufactured part in the layer as initial boundary $\delta\Omega$. The adaptive contour evolution is such that:

$$\frac{\delta\varphi(x,y,t)}{\delta t} = w(t)\delta_{region} + (1 - w(t))\delta_{edge} \quad \text{(A2)}$$

where δ_{region} represents the region-based term of the active contour formulation, δ_{edge} represents the edge-based term, and $w(t)$ is a weight to balance the influence of the region-based and edge-based terms in the convergence to the final reconstructed contour. The region-based term relies on the average difference of pixel intensity inside and outside the boundary to drive the shrink/expansion operations. Conversely, the edge-based term relies on pixel intensity gradients within the image to drive the iterative evolution of the reconstructed boundary. The weight $w(t)$ is such that $0 \leq w(t) \leq 1$. It is a function of the iteration counter, t, as higher weight is given to the region-based term in initial iterations for first rough segmentation, then a higher weight is given to the edge-based term in last iterations. This allows using the edge-based segmentation to refine and fine-tune the region-based one, aiming to achieve a more accurate reconstruction of actual boundaries. We refer the reader to Pagani et al. [14] for full details on the active contours segmentation technique.

Appendix B

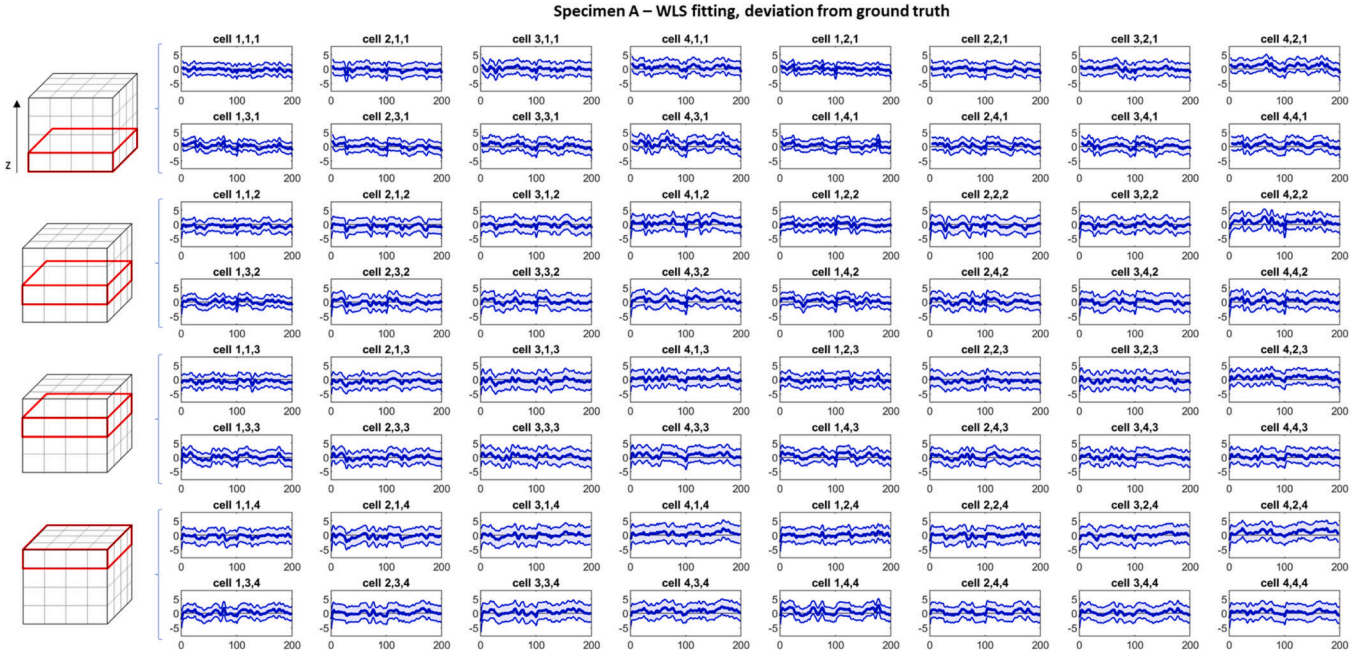

Fig. B1. WLS fitting with 95 % prediction intervals of the deviation from the ground truth for all unit cells of specimen A.

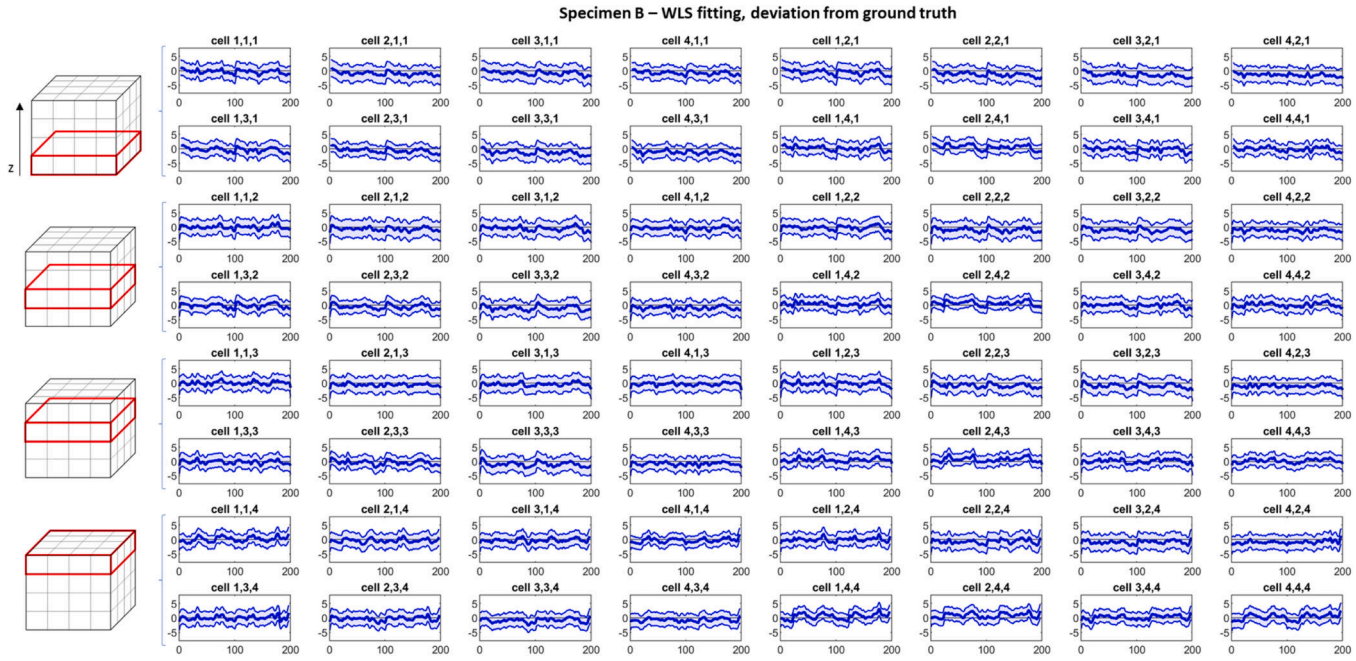

Fig. B2. WLS fitting with 95 % prediction intervals of the deviation from the ground truth for all unit cells of specimen B.

Data Availability

Data will be made available on request.

References

[1] M. Helou, S. Kara, Design, analysis and manufacturing of lattice structures: an overview, Int. J. Comput. Integr. Manuf. 31 (3) (2018) 243–261.

[2] X. Wu, Y. Su, J. Shi, Perspective of additive manufacturing for metamaterials development, Smart Mater. Struct. 28 (9) (2019) 093001.

[3] L. Liu, P. Kamm, F. Garcia-Moreno, J. Banhart, D. Pasini, Elastic and failure response of impefect three-dimensional metallic lattices: the role of geometric defects induced by Selective Laser Melting, Journal of the Mechanics and Physics of Solids 107 (2017) 160–184.

[4] D. Melancon, Z.S. Bagheri, R.B. Johnston, L. Liu, M. Tanzer, D. Pasini, Mechanical characterization of structurally porous biomaterials built via additive manufacturing: experiments, predictive models, and design maps for load-bearing bone replacement implants, Acta Biomater. 63 (2017) 350–368, https://doi.org/10.1016/j.actbio.2017.09.013.

[5] Donmez, A., Fox, J., Kim, F., Lane, B., Praniewicz, M., Tondane, V., Weaver, J., Witherell, P., (2024), In-process monitoring and non-destructive evaluation for metal additive manufacturing, NIST Internal Report, NIST IR 8538, https://doi.org/10.6028/NIST.IR.8538.

[6] M. Seifi, M. Gorelik, J. Waller, et al., Progress towards metal additive manufacturing standardization to support qualification and certification, JOM 69 (2017) 439–455, https://doi.org/10.1007/s11837-017-2265-2.

[7] M. Grasso, A. Remani, A. Dickins, B.M. Colosimo, R.K. Leach, In-situ measurement and monitoring methods for metal powder bed fusion: an updated review, Meas. Sci. Technol. 32 (11) (2021) 112001.

[8] R. McCann, M.A. Obeidi, C. Hughes, É. McCarthy, D.S. Egan, R.K. Vijayaraghavan, D. Brabazon, In-situ sensing, process monitoring and machine control in laser powder bed fusion: a review, Addit. Manuf. 45 (2021) 102058.

[9] Z. Snow, L. Scime, A. Ziabari, B. Fisher, V. Paquit, Scalable in situ non-destructive evaluation of additively manufactured components using process monitoring, sensor fusion, and machine learning, Addit. Manuf. 78 (2023) 103817.

[10] Aminzadeh, M., & Kurfess, T.. (2016, June). Vision-based inspection system for dimensional accuracy in powder-bed additive manufacturing. In International manufacturing science and engineering conference (Vol. 49903, p. V002T04A042). American Society of Mechanical Engineers.

[11] F. Caltanissetta, M. Grasso, S. Petro, B.M. Colosimo, Characterization of in-situ measurements based on layerwise imaging in laser powder bed fusion, Addit. Manuf. 24 (2018) 183–199.

[12] Gaikwad, A., Imani, F., Rao, P., Yang, H., & Reutzel, E. (2019, June). Design rules and in-situ quality monitoring of thin-wall features made using laser powder bed fusion. In International Manufacturing Science and Engineering Conference (Vol. 58745, p. V001T01A039). American Society of Mechanical Engineers.

[13] He, P., Zhong, K., Liu, X., Zhou, G., Wang, C., Wei, Q., … & Li, Z. (2019, October). A phase-guided method for extracting the contour of the fusion area in laser powder bed fusion. In Seventh International Conference on Optical and Photonic Engineering (icOPEN 2019) (Vol. 11205, p. 112051H). International Society for Optics and Photonics.

[14] L. Pagani, M. Grasso, P.J. Scott, B.M. Colosimo, Automated layerwise detection of geometrical distortions in laser powder bed fusion, Addit. Manuf. 36 (2020) 101435.

[15] J. zur Jacobsmühlen, J. Achterhold, S. Kleszczynski, G. Witt, D. Merhof, In situ measurement of part geometries in layer images from laser beam melting processes, Prog. Addit. Manuf. 4 (2) (2019) 155–165.

[16] B.M. Colosimo, M. Grasso, F. Garghetti, B. Rossi, Complex geometries in additive manufacturing: a new solution for lattice structure modeling and monitoring, J. Qual. Technol. 54 (4) (2022) 392–414.

[17] B.M. Colosimo, F. Garghetti, L. Pagani, M. Grasso, A novel method for in-process inspection of lattice structures via in-situ layerwise imaging, Manuf. Lett. 32 (2022) 67–72.

[18] M.G. Guerra, M. Lafirenza, V. Errico, A. Angelastro, In-process dimensional and geometrical characterization of laser-powder bed fusion lattice structures through high-resolution optical tomography, Opt. Laser Technol. 162 (2023) 109252.

[19] J.B. Forien, G.M. Guss, S.A. Khairallah, W.L. Smith, P.J. DePond, M.J. Matthews, N. P. Calta, Detecting missing struts in metallic micro-lattices using high speed melt pool thermal monitoring, Addit. Manuf. Lett. 4 (2023) 100112.

[20] J.O. Ramsay, B.W. Silverman, Functional Data Analysis, Springer, 2005.

[21] B.M. Colosimo, P. Cicorella, M. Pacella, M. Blaco, From profile to surface monitoring: SPC for cylindrical surfaces via Gaussian processes, J. Qual. Technol. 46 (2) (2014) 95–113.

[22] A. Menafoglio, M. Grasso, P. Secchi, B.M. Colosimo, Profile monitoring of probability density functions via simplicial functional PCA with application to image data, Technometrics 60 (4) (2018) 497–510.

[23] A. Wang, K. Wang, F. Tsung, Statistical surface monitoring by spatial-structure modeling, J. Qual. Technol. 46 (4) (2014) 359–376.

[24] Y. Zang, P. Qiu, Phase I monitoring of spatial surface data from 3D printing, Technometrics 60 (2) (2018) 169–180.

[25] Y. Zang, P. Qiu, Phase II monitoring of free-form surfaces: an application to 3D printing, J. Qual. Technol. 50 (4) (2018) 379–390.

[26] M. Abdelrahman, E.W. Reutzel, A.R. Nassar, T.L. Starr, Flaw detection in powder bed fusion using optical imaging, Addit. Manuf. 15 (2017) 1–11.

[27] C. Gobert, E.W. Reutzel, J. Petrich, A.R. Nassar, S. Phoha, Application of supervised machine learning for defect detection during metallic powder bed fusion additive manufacturing using high resolution imaging, Addit. Manuf. 21 (2018) 517–528.

[28] R. Szeliski, Image alignment and stitching. Computer Vision, Springer, Cham, 2022, pp. 401–441.

[29] B.B. Avants, N.J. Tustison, M. Stauffer, G. Song, B. Wu, J.C. Gee, The insight toolkit image registration framework, Front. Neuroinform. 8 (44) (2014).

[30] S. Liu, Y. Peng, A local region-based Chan–Vese model for image segmentation, Pattern Recognit. 45 (7) (2012) 2769–2779.

[31] S. Soomro, A. Munir, K.N. Choi, Hybrid two-stage active contour method with region and edge information for intensity inhomogeneous image segmentation, PloS One 13 (1) (2018) e0191827.
[32] S. Osher, R. Fedkiw, K. Piechor, Level set methods and dynamic implicit surfaces, Appl. Mech. Rev. 57 (3) (2004). B15-B15.
[33] Z. Li, X. Liu, S. Wen, P. He, K. Zhong, Q. Wei, S. Liu, In situ 3D monitoring of geometric signatures in the powder-bed-fusion additive manufacturing process via vision sensing methods, Sensors 18 (4) (2018) 1180.
[34] M.S. Nixon, A.S. Aguado, Feature extraction & image processing for computer vision, Academic Press, 2012.
[35] M. Bugatti, B.M. Colosimo, The intelligent recoater: a new solution for in-situ monitoring of geometric and surface defects in powder bed fusion, Addit. Manuf. Lett. 3 (2022) 100048.
[36] L. Tan Phuc, M. Seita, A high-resolution and large field-of-view scanner for in-line characterization of powder bed defects during additive manufacturing, Mater. Des. 164 (2019) 107562.
[37] D. Huang, S. Du, G. Li, C. Zhao, Y. Deng, Detection and monitoring of defects on three-dimensional curved surfaces based on high-density point cloud data, Precis. Eng. 53 (2018) 79–95.